



Pyrazolo[4,3-c]isoquinolines as potential inhibitors of NF- κ B activation

Jérémie Mortier^{a,1}, Raphaël Frederick^{a,1}, Corinne Ganef^b, Caroline Remouchamps^b, Patrice Talaga^c, Lionel Pochet^a, Johan Wouters^a, Jacques Piette^b, Emmanuel Dejardin^b, Bernard Masereel^{a,*}

^a Drug Design & Discovery Center, University of Namur, FUNDP, 61 Rue de Bruxelles, 5000 Namur Belgium

^b Laboratory of Virology and Immunology, GIGA Research, University of Liège, Belgium

^c UCB SA Belgium

ARTICLE INFO

Article history:

Received 4 November 2009

Accepted 12 January 2010

Keywords:

NF- κ B inducing kinase
TGF- β activated kinase 1
Pyrazoloisoquinolines
Alternative pathway
Rheumatoid arthritis
Molecular modeling

ABSTRACT

In this work, we aimed to build a 3D-model of NIK and to study the binding of pyrazolo[4,3-c]isoquinolines with a view to highlight the structural elements responsible for their inhibitory potency. However, in the course of this work, we unexpectedly found that the pyrazolo[4,3-c]isoquinolines initially reported as NIK inhibitors were neither inhibitors of this enzyme nor of the alternative NF- κ B pathway, but were in fact inhibitors of another kinase, the TGF- β activated kinase 1 (TAK1) which is involved in the classical NF- κ B pathway.

© 2010 Elsevier Inc. All rights reserved.

1. Introduction

Rheumatoid arthritis (RA) is a systemic autoimmune disease affecting around 1–2% of worldwide population. Patients with RA have an increased risk of early death. This pathology is mainly characterized by an uncontrolled proliferation and accumulation of inflammatory cells within the synovial fluids, causing cartilage and bone resorption. Many cell types contribute to the pathogenesis ranging from lymphocytes to stroma cells [1]. These cells express a panel of inflammatory mediators that activate multiple signaling pathways. Most of these signaling pathways lead to the activation of the transcription factor NF- κ B and MAPK cascade.

It was recently shown that two main pathways control the activation of NF- κ B. The first one, named classical NF- κ B pathway, is triggered by inflammatory cytokines such as TNF α or IL-1, or by bacterial and viral proteins through pathogen-recognition receptors (PRR) like TLRs and NLRs [2]. These inducers trigger the recruitment of specific adaptor proteins to their cognate receptors, which enable the activation of a cascade of kinases. Among them, TGF- β activated kinase 1 (TAK1) plays a key role at the crossroad of the NF- κ B and MAPK signaling pathways (Fig. 1). TAK1 was first discovered as a TGF- β activated kinase and is part of the MAP

kinase subfamily [3]. However, recent studies showed that IL-1 β and TNF α signaling pathways are affected in TAK1 KO mice [4,5]. TAK1 activates the IKK complex by phosphorylating the subunit IKK β and acts on MKK6 to trigger the activation of p38 and JNK (Fig. 1). Upon TAK1 activation, the IKK complex phosphorylates I κ B α , the main inhibitor of the classical NF- κ B pathway, releasing NF- κ B (e.g.; p50/p65), which finally, translocates into the nucleus [6]. This pathway is activated within minutes and relies on the indispensable adaptor protein NEMO, or IKK γ , holding together IKK β and IKK α to form the IKK complex.

The second NF- κ B pathway, called alternative NF- κ B pathway, is induced by a subset of TNFL family members as well as by some viral proteins [7]. This pathway is dependent on the stabilization and activation of the kinase NIK. The half-life of this particular kinase is negatively controlled by TRAF-2, TRAF-3, c-IAP-1 and c-IAP-2 [8,9]. Upon activation of receptors like CD40, BAFF or LT β R, the inhibitory function of TRAF-2 and -3 is alleviated. Then, stabilized NIK activates IKK α leading to the processing of p100 into p52 [10–12]. The latter, in association with its main partner Rel-B, fulfils non-redundant biological functions such as secondary lymphoid organ development and induction of specific chemokines involved in adaptive immunity [7].

Because a wide variety of pro-inflammatory cytokines play a role in the development of RA, it might be valuable to design a novel class of inhibitors targeting proteins at the crossroad of multiple pathways relevant to this pathology. Among the potential proteins, NIK certainly represents an attractive candidate since it is

* Corresponding author. Tel.: +32 81724338; fax: +32 4 81724299.
E-mail address: bernard.masereel@fundp.ac.be (B. Masereel).

¹ These authors equally contributed to this work.

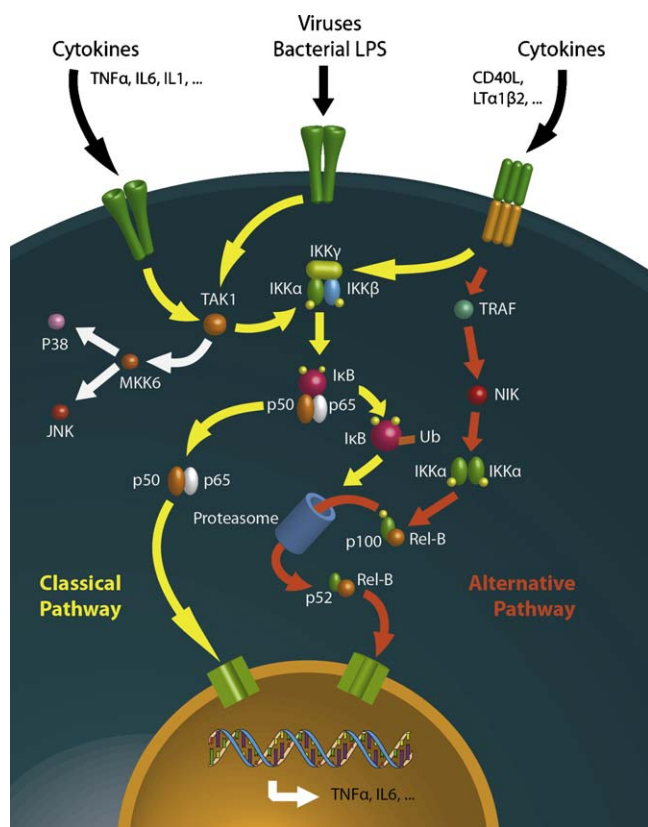


Fig. 1. Classical (yellow) and alternative (orange) NF- κ B activation pathways.

involved downstream of many TNFR like CD40, RANK or LT β R involved in the pathogenesis of RA.

According to our knowledge, presently only one series of compounds has been claimed as NIK inhibitors. These are characterized by a pyrazolo[4,3-*c*]isoquinoline ring substituted in position 1, 3, 5, 7 and 9 (Fig. 2) [13]. Most of the chemical modifications around the pyrazolo[4,3-*c*]isoquinoline template involved the introduction of bulky, lipophilic groups such as phenyl, trifluoromethylphenyl, pyridine or pentafluorophenyl in the 5-position and introduction of small lipophilic groups like a methyl or a trifluoromethyl in the 1- and 5-positions. Unfortunately, poor information was given in the original patent relating to their biological evaluation. For instance, the claimed NIK inhibitory potency is only based on a whole cellular assay in presence of some derivatives. No data on isolated NIK enzyme are available.

At a structural point of view, the 3D-structure of NIK has not yet been elucidated. The NIK amino acid sequence is comprised of 947 residues with a kinase domain containing 256 residues (400 to 655). Thus, the absence of any 3D-structure of this enzyme hindered the discovery of novel NIK inhibitors.

In this work, we aimed to build a 3D-model of NIK and to study the binding of the reported pyrazolo[4,3-*c*]isoquinolines with a

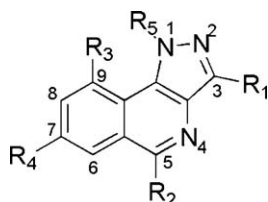


Fig. 2. Chemical structure of the pyrazolo[4,3-*c*]isoquinoline scaffold reported by Flohr as NIK inhibitors [13].

view to highlight the structural elements responsible for their inhibitory potency. This would help us to subsequently search for novel and more potent inhibitors of this enzyme using the gathered information.

However, in the course of this work, we unexpectedly found that the pyrazolo[4,3-*c*]isoquinolines initially reported as NIK inhibitors were neither inhibitors of this enzyme nor of the alternative NF- κ B pathway, but were in fact inhibitors of another kinase, the TGF- β activated kinase 1 (TAK1) which is involved in the classical NF- κ B pathway. This was confirmed by the re-synthesis and the enzymatic evaluation of representative pyrazolo[4,3-*c*]isoquinolines. These results strongly suggesting a completely different mechanism of action for the pyrazolo[4,3-*c*]isoquinolines in modulating the NF- κ B pathway, and allow to review the state-of-the-art of NIK inhibitors and should without any doubt be of value for scientists working in this field.

2. Material and methods

2.1. Homology modeling

The human M3K14 (NIK) sequence was obtained from the Swiss-Prot database (primary accession number Q99558). Sequence alignment was performed using *BLASTP* [14], through the Protein Data Bank (BLOSUM62 matrix) [15]. The human PAK1 (PDB code 1YHW_A) was selected as the most appropriate template, and amino acid sequences were then aligned by means of the *ESyPred3D* program [16]. Quality of the model has been analysed by means of PDBsum server, and the Ramachandran plot is available in supporting information [17]. To take into account protein flexibility, the resulting model was minimized using the *MINIMIZE* module included in *SYBYL* 8.0 program [18].

2.2. Docking simulations

Compounds **6a–s** were built using the *SKETCH* module, as implemented in *SYBYL* (version 8.0) [18], and their geometry was optimized using *MINIMIZE* module. The minimization process uses *POWELL* method with the *TRIPOS* force field (dielectric constant 1 r) to reach a final convergence of 0.01 kcal mol $^{-1}$. Docking simulation was then performed into the homology model of the human kinase NIK with the automated *GOLD* program. The active site was defined including all residues in a volume of 7 Å around 3-OH-staurosporine superimposed onto the model of NIK.

A similar procedure was used to dock **6d** inside the TAK1 binding cleft using the 3D-coordinates obtained from X-ray diffractions [19]. In the case of TAK1, the active site was defined by a sphere of 15 Å around residue A107 in the active site.

2.3. Chemistry

^1H NMR spectra were recorded at 20 °C in CDCl $_3$ or DMSO- d_6 on a 400 MHz Jeol Spectrometer (Jeol JNM EX-400). Chemical shifts are reported in δ ppm relative to tetramethylsilane (TMS) as a singlet at 0 ppm (δ). Thin-layer chromatography (TLC) was performed on aluminum supported 0.25 mm silica gel plates (Merck 5719, 250 meshes). TLC plates were visualized under 254 nm and 320 nm UV light. Elemental analyses (C, H, N) were performed on a Thermo Finnigan FlashEA 1112 apparatus. Mass spectra were recorded on an 1100 series MSD Trap spectrometer equipped with an electrospray ionization (ESI) source. Flash chromatography purifications were performed on a Biotage SP1 Purification System using silica or C18 Biotage FLASH+ $^{\text{®}}$ Cartridges. Microwave assisted reactions were performed using an Initiator 16 Single-mode Microwave system producing a 2.450 GHz controlled irradiation (Biotage AB, Uppsala). The

temperature was measured with an IR sensor on the outside of the reaction vial.

The purity of compounds **6a–d** was also verified by LC on an Agilent 1100 series system. System control, data collection and data processing were accomplished using ChemStation software (Agilent Technologies, Santa Clara). The mobile phase contained acetonitrile and acetic acid (0.1%). Compounds were detected and their purity was calculated using a UV detector (wavelength: 240 nm). Two different methods were used to analyse the reported compounds. Method 1: injection volume = 3 μ L in acetonitrile; gradient elution from 5% to 95% of acetonitrile over 2.4 min, then 95% acetonitrile until 3.6 min; analytical column C8 Zorbax Eclipse Plus (4.6 mm \times 50 mm, 1.8 μ m particle size); flowrate = 1.25 mL min⁻¹; 1; temperature = 40 °C. Method 2: injection volume = 5 μ L in acetonitrile; gradient elution from 5% to 95% of acetonitrile over 4.5 min, then 95% acetonitrile until 8.0 min; analytical column C18 Zorbax SB column (3.0 mm \times 100 mm, 3.5 μ m particle size); flowrate = 0.5 mL min⁻¹; temperature = 40 °C. Retention times were reported as *Rt*₁ and *Rt*₂ for these two methods respectively.

2.3.1. 1,3-Diphenyl-propane-1,2,3-trione 2-oxime **2b**

240 mg (3.46 mmol) of sodium nitrite were dissolved in water (2 mL) and added dropwise to a solution of 130 mg (0.58 mmol) of dibenzoylmethane **1b** diluted into acetic acid (10 mL). At room temperature, the solution was stirred for 1 h. The reaction mixture was extracted three times with diethyl ether (20 mL). The organic layers were combined and washed with a saturated aqueous solution of sodium bicarbonate (30 mL). Solvents were evaporated under reduced pressure, and the crude product purified by flash chromatography to give the title compound (Silica column; Eluant AcOEt: cyclohexane with gradient from 8% to 30% of AcOEt over 30 min; Flowrate 40 mL min⁻¹). Yield: 81%. ¹H RMN (DMSO-*d*₆, 400 MHz): δ = 7.52–7.58 (m, 4H, *H*_{arom}), 7.68 (t, 2H, *H*_{arom}), 7.82 (d, 2H, *H*_{arom}), 7.99 (d, 2H, *H*_{arom}). Anal. Calcul. for C₁₅H₁₁NO₃: C, 71.14; H, 4.38; N, 5.53. Found: C, 71.29; H, 4.62; N, 5.23. *m/z* 254.0 [M + H]⁺, 276.1 [M + Na]⁺

2.3.2. 4-Amino-3-methyl-5-phenyl-1H-pyrazole **3a**

At 0 °C, hydrazine hydrate (0.18 mL, 3.70 mmol) was added dropwise to a solution of 1-phenylbutane-1,2,3-trione-2-oxime **2a** (0.37 mmol) in ethanol (4 mL). Then, the mixture was stirred for 7 h at room temperature. Solvents were removed under reduced pressure and the crude product diluted in ethyl acetate (10 mL). The solution was acidified by HCl 3N (15 mL) and the organic layer discarded. The aqueous layer was neutralized by NaOH 1N (50 mL) and extracted with ethyl acetate (3 \times 20 mL). The organic layers were combined, dried, and the solvent evaporated under reduced pressure. The crude product was purified by flash chromatography (Silica column; eluant: AcOEt:cyclohexane from 20% to 100% of AcOEt over 45 min; flowrate: 40 mL min⁻¹). Yield: 86%. ¹H RMN (CDCl₃, 400 MHz): δ = 2.37 (s, 3H, CH₃), 7.31 (t, 1H, *H*_{arom}), 7.42 (t, 2H, *H*_{arom}), 7.61 (d, 2H, *H*_{arom}). Anal. Calcul. for C₁₀H₁₁N₃: C, 69.34; H, 6.40; N, 24.26. Found: C, 69.30; H, 6.14; N, 23.56. *m/z* 174.1 [M + H]⁺.

2.3.3. 4-Amino-3,5-diphenyl-1H-pyrazole **3b**

The title compound was synthesized with the same procedure than that used for **3a**. Yield: 88%. ¹H RMN (CDCl₃, 400 MHz): δ = 7.25 (t, 2H, *H*_{arom}), 7.48 (t, 4H, *H*_{arom}), 7.68 (d, 4H, *H*_{arom}). Anal. Calcul. for C₁₅H₁₃N₃: C, 76.57; H, 5.57; N, 17.86. Found: C, 76.27; H, 5.65; N, 17.62. *m/z* 236.2 [M + H]⁺.

2.3.4. 4-Benzamido-3,5-diphenyl-1H-pyrazole **5a**

Benzoic acid **4a** (92.6 mmol), hydroxybenzotriazole (HOBt; 185 mmol) and *N*-(3-dimethylaminopropyl)-*N'*-ethylcarbodiimide (DEC; 79.5 mmol) were added to 4-amino-3,5-diphenyl-

1H-pyrazole **3b** (92.6 mmol) diluted in dichloromethane (30 mL). Two drops of BMimpF₆ were added, and the mixture was heated in the microwave oven for 1 h (70 °C). Then, water (20 mL) was added and the mixture extracted by ethyl acetate (3 \times 20 mL). The organic layers were combined, dried, and the solvent evaporated under reduced pressure. The crude product was purified by flash chromatography (Silica column; Eluant: AcOEt:cyclohexane from 20% to 71% of AcOEt over 40 min; flowrate: 40 mL min⁻¹). Yield: 60%. ¹H RMN (CDCl₃, 400 MHz): δ = 7.28–7.46 (m, 6H, *H*_{arom}), 7.49 (t, *J* = 7.3 Hz, 2H, *H*_{arom}), 7.56 (t, *J* = 7.3 Hz, 1H, *H*_{arom}), 7.64 (d, *J* = 6.3 Hz, 2H, *H*_{arom}), 7.72 (d, *J* = 6.3 Hz, 2H, *H*_{arom}), 7.92 (d, *J* = 7.3 Hz, 2H, *H*_{arom}), 9.96 (s, 1H, HN_{amide}). Anal. Calcul. for C₂₂H₁₇N₃O₂: C, 73.93; H, 5.36; N, 11.76. Found: C, 74.03; H, 5.13; N, 11.42. *m/z* 340.2 [M + H]⁺, 362.2 [M + Na]⁺.

2.3.5. 4-(3-Methoxybenzamido)-3,5-diphenyl-1H-pyrazole **5b**

The title compound was synthesized from 3-methoxybenzoic acid **4b** and 4-amino-3,5-diphenyl-1H-pyrazole **3b** as starting material, and according to the same procedure than that described for **5a**. Yield: 60%. ¹H RMN (DMSO-*d*₆, 400 MHz): δ = 3.77 (s, 3H, OCH₃), 7.12 (d, *J* = 8.2 Hz, 1H, *H*_{arom}), 7.26–7.45 (m, 8H, *H*_{arom}), 7.52 (d, *J* = 7.3 Hz, 1H, *H*_{arom}), 7.64 (d, *J* = 7.3 Hz, 2H, *H*_{arom}), 7.72 (d, *J* = 7.3 Hz, 2H, *H*_{arom}), 9.94 (s, 1H, HN). Anal. Calcul. for C₂₃H₁₇N₃O₂: C, 78.61; H, 4.88; N, 11.96; O, 11.58. Found: C, 78.04; H, 5.19; N, 11.58. *m/z* 369.2 [M + H]⁺, 391.3 [M + Na]⁺.

2.3.6. 4-(3-Methoxybenzamido)-3-methyl-5-phenyl-1H-pyrazole **5c**

The title compound was synthesized from 3-methoxybenzoic acid **4b** and 4-amino-3-methyl-5-phenyl-1H-pyrazole **3a** as starting material, and according to the same procedure than that described for **5a**. Yield: 57%. ¹H RMN (DMSO-*d*₆, 400 MHz): δ = 2.08 (s, 3H, CH₃), 3.78 (s, 3H, OCH₃), 7.12 (d, *J* = 8.2 Hz, 1H, *H*_{arom}), 7.22–7.41 (m, 4H, *H*_{arom}), 7.49 (s, 1H, *H*_{arom}), 7.54 (d, *J* = 7.5 Hz, 1H, *H*_{arom}), 7.6–7.7 (m, 2H, *H*_{arom}), 9.69 (s, 1H, HN). Anal. Calcul. for C₁₈H₁₇N₃O₂: C, 70.34; H, 5.58; N, 13.67. Found: C, 70.51; H, 5.35; N, 13.36. *m/z* 308.2 [M + H]⁺.

2.3.7. 4-Benzamido-3-methyl-5-phenyl-1H-pyrazole **5d**

The title compound was synthesized from benzoic acid **4a** and 4-amino-3-methyl-5-phenyl-1H-pyrazole **3a** as starting material, and according to the same procedure than that described for **5a**. Yield: 75%. ¹H RMN (CDCl₃, 400 MHz): δ = 2.26 (s, 3H, CH₃), 7.34–7.51 (m, 6H, *H*_{arom}), 7.61 (d, *J* = 8.2 Hz, 2H, *H*_{arom}), 7.71 (d, *J* = 7.5 Hz, 1H, *H*_{arom}), 7.83 (d, *J* = 8.2 Hz, 1H, *H*_{arom}). Anal. Calcul. for C₁₇H₁₅N₃O₂: C, 71.31; H, 5.63; N, 14.68. Found: C, 72.07; H, 5.33; N, 14.53. *m/z* 278.1 [M + H]⁺.

2.3.8. 3,5-Diphenyl-1H-pyrazolo[4,3-*c*]isoquinoline **6a**

4-Benzamido-3,5-diphenyl-1H-pyrazole **5a** (0.36 mmol) and phosphorus pentoxide (3.60 mmol) were suspended in dry chlorobenzene (10 mL) and *N,N*-diethylaniline (0.36 mmol). Under argon atmosphere, the mixture was warmed up to 120 °C and phosphorus oxychloride (0.54 mmol) was added dropwise. The temperature was maintained for 24 h. At the end, a saturated solution of sodium bicarbonate (10 mL) was carefully added, and the mixture was extracted by dichloromethane (3 \times 20 mL). The organic layers were combined, dried on magnesium sulfate and the solvent was evaporated under reduced pressure. The crude product was purified by preparative HPLC (C18 column and isocratic mobile phase MeCN: AcOH 0.1% 50:50) to give the title compound **6a**. Yield: 2%. *m/z* 340.2 [M + H]⁺, 362.2 [M + Na]⁺. ¹H RMN (CDCl₃, 400 MHz): δ = 7.35 (t, *J* = 7.5, 1H, *H*_{arom}), 7.46–7.71 (m, 9H, *H*_{arom}), 7.97 (t, *J* = 8.2 Hz, 1H, *H*_{arom}), 8.04 (d, *J* = 7.5 Hz, 1H, *H*_{arom}), 8.51 (d, *J* = Hz, 2H, *H*_{arom}). *Rt*₁ = 3.35 min; *Rt*₂ = 7.49 min *m/z* 352.2 [M + H]⁺.

2.3.9. 5-(3-Methoxyphenyl)-3-phenyl-1H-pyrazolo[4,3-c]isoquinoline **6b**

The title compound was synthesized from 4-(3-methoxybenzamido)-3,5-diphenyl-1H-pyrazole **5b** as starting material and according to the procedure described for compound **6a**. Yield: 7%. ¹H RMN (CDCl₃, 400 MHz): δ = 3.81 (s, 3H, OCH₃), 7.11 (dd, *J*₁ = 2.2 Hz, *J*₂ = 8.1 Hz, 1H, H_{arom}), 7.20–7.24 (m, 1H, H_{arom}), 7.21 (d, *J*₁ = 2.2 Hz, 1H, H_{arom}), 7.35 (t, *J* = 7.3 Hz, 1H, H_{arom}), 7.46–7.50 (m, 3H, H_{arom}), 7.70 (t, *J* = 7.7 Hz, 1H, H_{arom}), 7.95 (t, *J* = 7.7 Hz, 1H, H_{arom}), 8.06 (d, *J* = 8.4 Hz, 1H, H_{arom}), 8.52–8.50 (m, 3H, H_{arom}). *Rt*₁ = 3.30 min; *Rt*₂ = 7.38 min *m/z* 352.2 [M + H]⁺.

2.3.10. 5-(3-Methoxyphenyl)-3-methyl-1H-pyrazolo[4,3-c]isoquinoline **6c**

The title compound was obtained from 4-(3-methoxybenzamido)-3-methyl-5-phenyl-1H-pyrazole **5c** as starting material and according to the procedure described for compound **6a**. Yield: 6%. ¹H RMN (CDCl₃, 400 MHz): δ = 2.76 (s, 3H, CH₃), 3.87 (s, 3H, OCH₃), 7.03 (d, *J* = 10.8 Hz, 1H, H_{arom}), 7.21–7.28 (m, 2H, H_{arom}), 7.44 (t, *J* = 12.1 Hz, 1H, H_{arom}), 7.59 (t, *J* = 10.8 Hz, 1H, H_{arom}), 7.81 (t, *J* = 10.8 Hz, 1H, H_{arom}), 8.13 (d, *J* = 12.1 Hz, 1H, H_{arom}), 8.22 (d, *J* = 12.1 Hz, 1H, H_{arom}). *Rt*₁ = 2.78 min; *Rt*₂ = 6.15 min. *m/z* 289.3 [M + H]⁺.

2.3.11. 3-Methyl-5-phenyl-1H-pyrazolo[4,3-c]isoquinoline **6d**

The title compound was synthesized from 4-benzamido-3-methyl-5-phenyl-1H-pyrazole **5d** as starting material and according to the procedure described for compound **6a**. Yield: 13%. ¹H RMN (CDCl₃, 400 MHz): δ = 2.76 (s, 3H, CH₃), 7.51–7.60 (m, 4H, H_{arom}), 7.68 (d, *J* = 7.5 Hz, 2H, H_{arom}), 7.78 (t, *J* = 7.5 Hz, 1H, H_{arom}), 8.10 (d, *J* = 8.5 Hz, 1H, H_{arom}), 8.22 (d, *J* = 7.5 Hz, 1H, H_{arom}). *Rt*₁ = 2.78 min; *Rt*₂ = 6.15 min. *m/z* 260.1 [M + H]⁺.

2.4. NIK enzymatic assay

This experiment was performed by ProQinase using 33PanQinase[®] technology [31]. Inhibitory potency of staurosporine and molecules **6a–d** were evaluated on human recombinant NIK. DMSO was used as cosolvent and its final concentration was 1%. NIK was expressed in Sf9 insect cells as human recombinant GST-fusion protein. The kinase was purified by affinity chromatography using GSH-agarose. The purity of the kinase was checked by SDS-PAGE/silver staining and the identity was verified by mass spectroscopy. The NIK activity was measured as the incorporation on an artificial substrate of ³³P produced by hydrolysis of [γ-³³P]-ATP. The substrate (RBER-CHKtide) was an artificial fusion protein expressed in *Escherichia coli*. It was consisting of a N-terminal GST-tag separated by a thrombin cleavage site from a fragment of the human retinoblastoma protein RB1, amino acids S773–K928 followed by 11 Arg residues (ER) and a peptide sequence KKKVRSGLYRSPSPENLNRP (CHKtide).

2.5. Alternative pathway assay

Human LTβR-positive HeLa cells have been used to evaluate the NIK inhibitory potency expressed as the inhibition of the processing of p100 into p52. Briefly, HeLa cells were cultured in DMEM with 10% FBS and plated in 6 well plates until they reach 80% of confluence. The cells were washed twice with PBS and incubated for 2 h with Opimem-1 containing 10, 20 or 50 μM of inhibitors. DMSO was used as cosolvent at a maximal concentration of 0.5% (v/v). At this concentration, DMSO has no effect. Then, an antibody acting as agonist of human LTβR (R&D Systems, Inc.) was added for 5 h. Afterwards, the cells were washed twice with PBS and lysed in SDS 0.5% containing a cocktail of protease and phosphatase inhibitors (Complete and PhosStop, Roche). Protein

extracts were quantified (Micro BCA protein kit assay, Pierce) and equal amounts of protein (15 μg) were loaded on SDS-PAGE for analyzing the processing of p100 into p52. For detecting p100 and p52, an antibody anti-human p52 (Upstate Cell Signaling 05-361) was used and a goat anti-mouse HRP (DAKO) was used as secondary antibody prior to measurement of the signal by chemiluminescence using the ECL kit from Pierce.

2.6. Multikinase assay

KinaseProfiler[™] is a millipore technology using standard protocole.

2.7. TAK1 enzymatic assay

This experiment was performed by Invitrogen using LanthaScreen[®] Kinase Binding Assay technology [32]. The test compounds were screened in 1% DMSO as final concentration. 3-fold serial dilutions were conducted from the starting concentration. All kinase/antibody mixtures were diluted to a 2× working concentration in the appropriate kinase buffer. The 4× AlexaFluor[®] labeled tracer was prepared in kinase buffer and the read out was on fluorescence plate reader.

2.8. Classical pathway assay

HeLa cells were cultured in DMEM with 10% FBS and plated in 6 well plates until they reach 80% of confluence. The cells were washed twice with PBS and incubated for 2 h with Opimem-1 containing 50 μM of inhibitor or DMSO alone. Then, TNF-α (Pepro Tech Inc.) was added at 100 U/mL for 0, 1 or 2 h. Total RNA samples were isolated with the Tripure reagent (Roche Molecular Biochemicals). One microgram of RNA was submitted to reverse transcription using M-MLV reverse transcriptase and random primers (Invitrogen) in a total volume of 20 μL. Two microliters of cDNA were submitted to real-time PCR using TaqMan 7000 SDS (Applied Biosystems) and SYBR Green detection (Eurogentec). The results were normalized with the 18S transcript. PCR was performed with the following primers for the following human transcript: *il-6*: FW 5'-CCAGGAGCCAGCTATGAAC-3' and RV 5'-CCCAGGGAGAAAGGCAACTG-3', *TNFα*: FW 5'-GGAGAAGGGTGACCGACTCA-3' and RV 5'-TGCCAGACTCGGCAAAG-3' and *18S*: FW 5'-AACTTTCGATGGTAGTCGCCG-3' and RV 5'-CCTTGGATGTGGTAGCCGTTT-3'.

3. Results

3.1. Building of a 3D-model of NIK

Since no experimentally-derived structural data for NIK were reported to date, a molecular model of this enzyme was first developed using comparative modeling. This technique comprises four main steps: (i) identification of a template, i.e. a protein of known 3D-structure that shares sequence homology with the target protein, (ii) alignment of the sequences of the target and template, (iii) building and optimization of the 3D-model and finally, (iv) quality assessment of the resulting structure. Following a BLASTP alignment, we identified the protein PAK1 (p21 activated kinase 1; PDB code: 1YHW_A) [20] as the best template. This protein shares 30% sequence identity and up to 48% sequence homology (similar residues) with NIK. As the target/template alignment step is known to be critical to the quality of the models, we used the automated homology program ESyPred3D [16]. This performs a consensus alignment between the sequences of the target, the template and other homologous proteins with the help of several different alignment algorithms and then uses MODELLER

[21] to generate the 3D-coordinates. The overall quality of the resulting models was finally evaluated using different methods. Ramachandran plots (available as Supporting Information) proved to be very satisfactory with 90.2% residues located in the most favored regions, 7.3% in the allowed regions, only four residues (1.6%) in the generously allowed regions (Phi and Psi torsion angles slightly larger than usual) and two residues in the disallowed regions (unfavorable Phi and Psi torsion angles). It should be noted that these six residues (Q484, T401, Y391, E395, D544 and S572) are located far from the active site and the hinge region.

A superimposition of NIK with PAK1 (Fig. 3) shows that the overall folding pattern (β -sheets, helices and main loops) is well preserved. The ATP-binding site region is also highly preserved. First, active site residues common to all serine–threonine kinases were identified. In the NIK structure, M469, which corresponds to M344 in PAK1, was identified as the gatekeeper (gk) residue. It is one of the essential residues in the ATP-binding site. Indeed, the nature of the gatekeeper (size and volume of the side-chain) is variable from one kinase to another, thus dictating the access to a specific pocket of the ATP-binding site (specificity pocket). Then, residues E470 (gk + 1) and L472 (gk + 3) which correspond to residues E345 and L347 in PAK1, were respectively identified in the hinge region [22]. These two residues are responsible for the stabilization of the adenine moiety of ATP. In the co-crystal structure of the complex between PAK1 and 3-OH-staurosporine (PDB code 2HY8), both residues are involved in the stabilization of the aromatic ring of 3-OH-staurosporine. Finally, in the back of the active site cavity, a salt bridge between residues K429 and E440 corresponding to the salt bridge between R299 and E315 in PAK1 is also highly preserved.

The catalytic pocket of NIK was refined by minimization to take into account the protein flexibility. The position of the side-chains of the residues located 20 Å around L472 were minimized by mean of the MINIMIZE module as implemented in SYBYL 8.0 [18].

To appraise the reliability of our model, the binding of the previously reported pyrazolo[4,3-*c*]isoquinolines was studied within the modeled active site. Staurosporine, which is known as a pankinase inhibitor including NIK [24] was also studied in our model. At a structural point of view, staurosporine is far from the template of the synthesized pyrazolo[4,3-*c*]isoquinolines.

3.2. Docking of pyrazolo[4,3-*c*]isoquinolines into the 3D-model of NIK

The pyrazolo[4,3-*c*]isoquinolines **6a–s** (Table 1) and staurosporine were docked inside the ATP-binding site of NIK using the automated GOLD program [25]. For each molecule, 20 conformations were generated and further evaluated following two

parameters: (i) the number of different orientations adopted by one molecule inside the NIK binding cleft and (ii) the number of different orientations where the compound is found to be stabilized with at least one H-bond with the residue L472 in the hinge region.

Interestingly, staurosporine fits perfectly the catalytic pocket, adopting a similar binding orientation as observed for 3-OH-staurosporine in PAK1 (Fig. 3). All of the 20 conformations generated lie in the same orientation with two H-bonds between the lactam ring of staurosporine and the NH and CO moieties of L472 and E470, respectively, stabilizing the moiety (Fig. 4a and b). In addition, hydrophobic interactions with aliphatic residues L406, V414, A427, L522 and C533 (not shown here for clarity) also contribute to the stabilization on both sides of the aromatic plane.

Conversely, when pyrazolo[4,3-*c*]isoquinolines **6a–s** are docked inside the ATP-binding site of NIK, several different orientations (2–6) were observed for each compound (Table 1), except for **6f** and **6r** for which a unique binding orientation of the pyrazolo[4,3-*c*]isoquinoline motif was found. But these two compounds did not interact with L472 through an H-bond as requested. In addition, in some cases, the inhibitor is not stabilized through H-bond interaction(s) with the hinge region residue L472. This interaction was however shown to be critical for kinase inhibition [22]. To see if an unique orientation could be highlighted, compounds **6a–s** were docked again inside the NIK binding cleft imposing a H-bond between the NH of L472 and one acceptor atom of the ligand. By doing so, two orientations (orientation 1 and orientation 2) were found as illustrated in Fig. 4 using compound **6d** as an example (Fig. 4c and d for orientation 1, and Fig. 4e and f for orientation 2). Although in both orientations the pyrazolo[4,3-*c*]isoquinoline scaffold is well stabilized by two H-bonds in the hinge region (as expected following a constraint docking), none of these two orientations seems more plausible than the other or would allow a better understanding of the structure–activity relationships in this series. Thus, this docking study does not allow to highlight an unique, obvious orientation of compounds **6a–s** into the NIK binding cavity.

Based on these observations, different hypothesis could be suggested: (i) although staurosporine, a true NIK inhibitor (discussed later), fits perfectly its active site, the 3D-model of NIK is not reliable, (ii) the pyrazolo[4,3-*c*]isoquinolines **6a–s** are effectively NIK inhibitors but through a different mechanism of inhibition, for instance through interaction with an allosteric site or (iii) the pyrazolo[4,3-*c*]isoquinolines are devoid of NIK inhibitory potency. To assess this assumption, some representative pyrazolo[4,3-*c*]isoquinolines (**6a–d**) were synthesized and their NIK inhibitory potency evaluated on isolated human recombinant

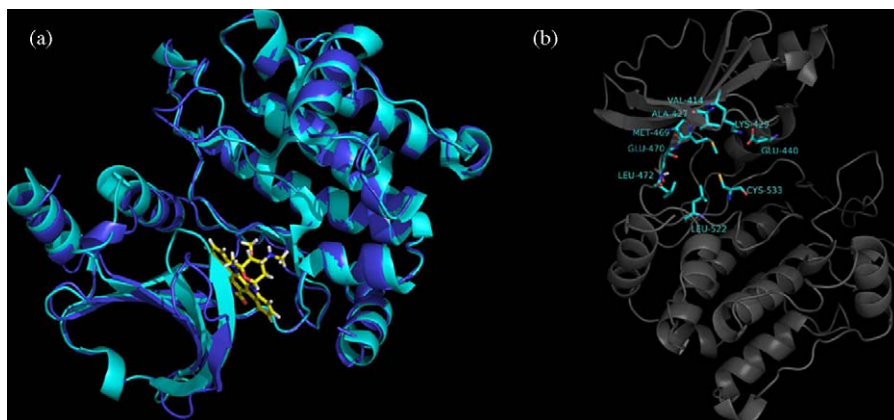


Fig. 3. (a) Superimposition of PAK1 (cyan) with 3-OH-staurosporine (yellow) and NIK (blue) and (b) view of NIK with main active site residues in cyan. Pictures made using PYMOL [23].

Table 1Structure and docking results for the pyrazolo[4,3-c]isoquinolines **6a–s**.

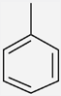
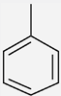
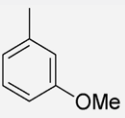
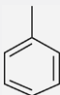
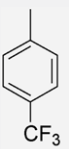
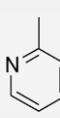
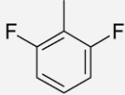
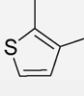
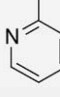
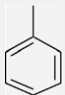
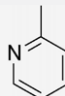
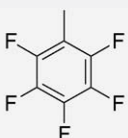
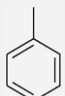
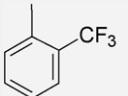
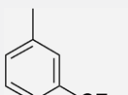
Cmpd	R ₁	R ₂	R ₃	R ₄	R ₅	Docking	
						Number of different orientations	Number of different orientations with H-bond with L472
Staurosporine						1	1
6a			H	H	H	4	1
6b			H	H	H	6	2
6c	Me		H	H	H	2	0
6d	Me		H	H	H	2	0
6e	Me		H	H	H	3	0
6f	Me		H	H	Me	1	0
6g	CF ₃		H	H	H	2	0
6h	Me		H	H	Me	2	1
6i	Me		H	COOMe	H	4	2
6j	Me		H	COOMe	H	3	2
6k	Me		H	H	Me	3	0
6l	Me		H	NMe ₂	H	2	0

Table 1 (Continued)

Cmpd	R ₁	R ₂	R ₃	R ₄	R ₅	Docking	
						Number of different orientations	Number of different orientations with H-bond with L472
6m	Me		CF ₃	H	H	2	1
6n	Me		CF ₃	H	H	4	2
6o	Me		H	H	H	4	1
6p	Me		H	NMe ₂	H	3	2
6q	Me		H	H	H	4	1
6r	Me		H	H	H	1	0
6s	Me	CH ₂ OMe	H	H	H	5	1

enzyme as well as on HeLa cells where the NF- κ B alternative pathway was induced.

3.3. Chemistry

The pyrazolo[4,3-c]isoquinolines **6a–d** were synthesized in four steps (Scheme 1). Starting from the commercially available diketones **1a–b**, oximes **2a–b** were prepared with a high yield by reaction of sodium nitrite in acidic conditions [26]. The oximes **2a–b** further reacted with hydrazine hydrate to form pyrazoles **3a–b** [26,27]. Then, benzoic acids **4a–b** activated by HOBT/DEC were condensed on pyrazoles **3a–b** to form the corresponding amides **5a–d**. Finally, the desired pyrazolo[4,3-c]isoquinolines **6a–d** (Table 1) were obtained according to the Pictet-Gams reaction in poor yields due to the formation of several side products during the reaction (Scheme 1) [28].

3.4. Biological evaluation

The NIK inhibitory potency of the prepared pyrazolo[4,3-c]isoquinolines (**6a–d**) was evaluated in two enzymatic systems (i) isolated human recombinant NIK and (ii) cultured HeLa cells where the alternative NF- κ B pathway was induced by an LT β R agonist antibody.

3.4.1. Human recombinant NIK inhibition

A radiometric protein kinase assay was used to measure the residual activity of NIK in presence of the synthesized inhibitors at a single concentration of 10 μ M. Briefly, NIK was expressed in Sf9

insect cells as human recombinant GST-fusion protein and purified by affinity chromatography using GSH-agarose. The substrate, a recombinant protein kinase (RBER-CHKtide) was also expressed in *E. coli*. The assay cocktails were incubated at 30 °C for 60 min with [γ -³³P]-ATP (1 μ M, pH 7.5). Incorporation of ³³P was measured with a microplate scintillation counter. Staurosporine was chosen as Ref. [24].

Although the inhibition of NIK in the presence of staurosporine was >70%, none of the pyrazoloisoquinolines **6a–d** significantly reduced NIK activity at 10 μ M (Table 2). This corroborates the modeling study and demonstrates that the pyrazolo[4,3-c]isoquinolines **6a–d** are not NIK inhibitors.

To confirm that these molecules could not inhibit other proteins of the NF- κ B alternative pathway, their inhibition property was then investigated in a cellular assay where the alternative pathway is solely involved.

3.4.2. NF- κ B alternative pathway inhibition

Briefly, pyrazolo[4,3-c]isoquinolines **6a–d** were assayed using carcinoma HeLa cells expressing LT β R. The NF- κ B alternative pathway was induced or not by an LT β R agonist antibody. After induction, NIK was overexpressed and the processing of p100 into p52 was triggered by phosphorylation of IKK α (Fig. 1). The p100/p52 ratio was finally analysed by Western blot. DMSO, used as cosolvent, has no effect. The results are reported on Fig. 5.

Staurosporine which strongly inhibit isolated human recombinant NIK also blocks this pathway (Fig. 5). Here again, none of the pyrazolo[4,3-c]isoquinolines **6a–d** inhibited the NF- κ B alternative pathway. In fact, the processing of p100 into p52 was observed in

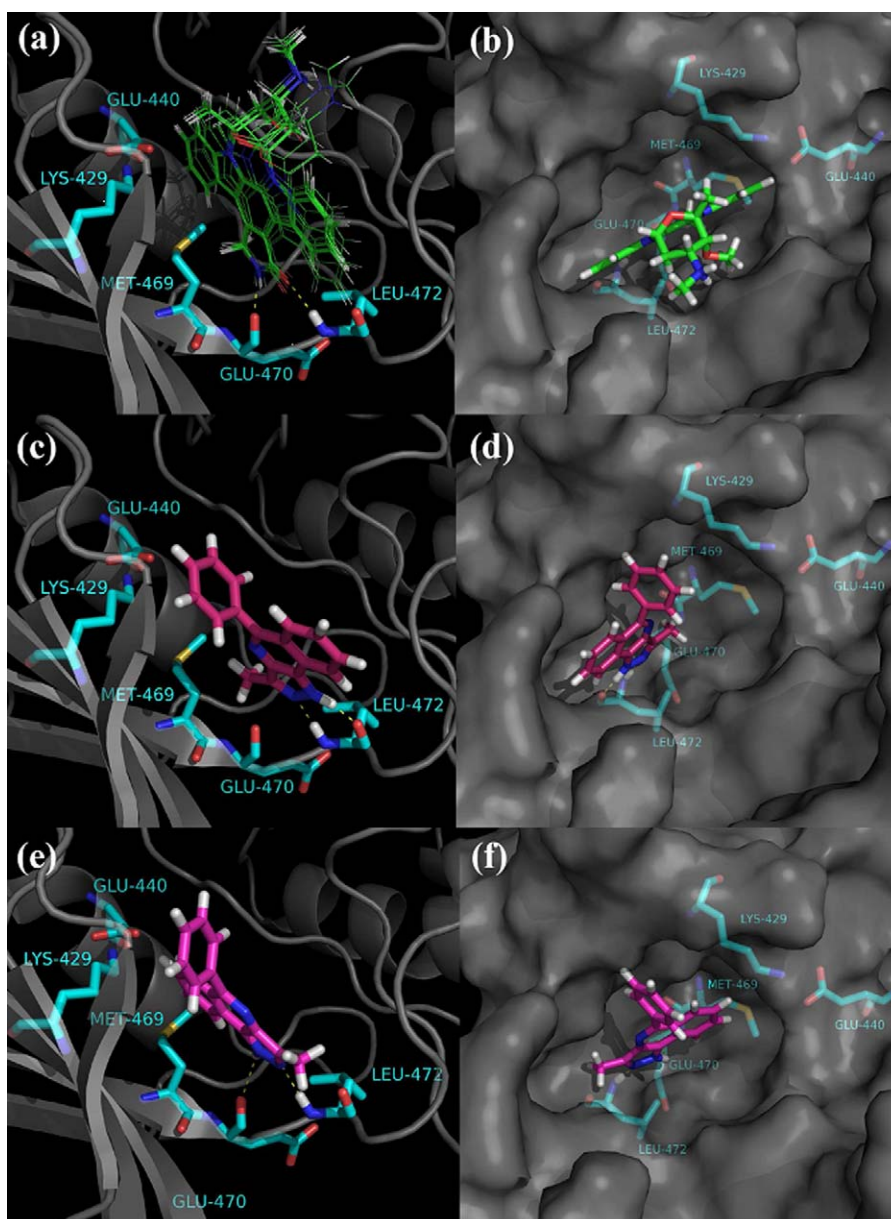


Fig. 4. (a) All of the 20 conformations obtained for staurosporine; (b) view of staurosporine in the active site cavity of NIK illustrated with the Connolly surface; (c and d) view of **6d** in the orientation 1 and (e and f) view of **6d** in the orientation 2 inside the NIK binding cleft. Pictures made using PYMOL [23].

the presence (+) and in the absence (–) of **6a–d** whatever the concentration of the inhibitor used (10, 20 or 50 μM). On the contrary to the claims of the original patent, the pyrazolo[4,3-*c*]isoquinolines **6a–d** cannot be considered as NIK inhibitors neither as blockers of the NF- κB alternative pathway.

3.4.3. Multikinase assay

With the aim to identify the putative target of the pyrazolo[4,3-*c*]isoquinolines, a multikinase screening assay was performed. The pyrazolo[4,3-*c*]isoquinoline **6d** was selected to carry out this study. The inhibitory properties of **6d** were thus evaluated on a panel of 263 kinases (Millipore KinaseProfiler™) at 10 μM .

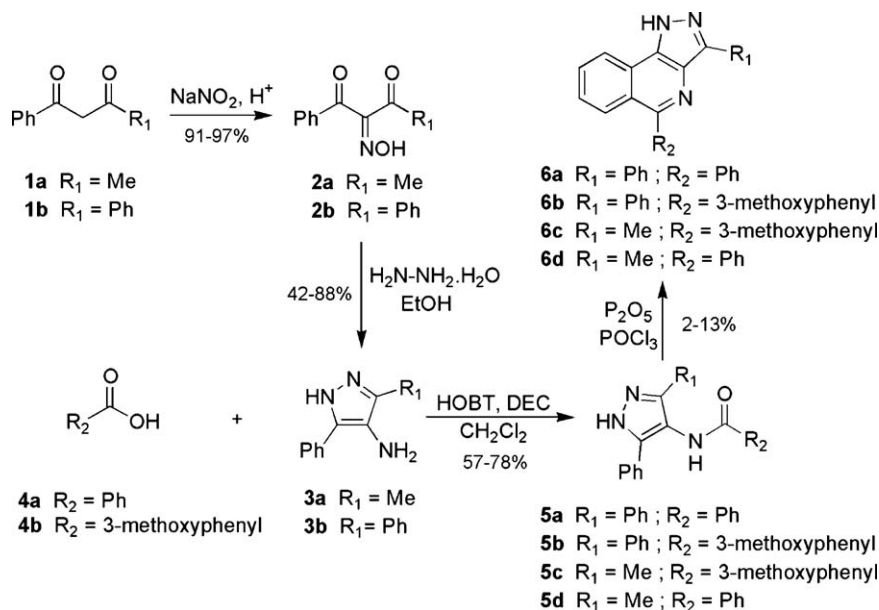
As a result, an inhibition of at least 50% was observed for 92 kinases over the 263 kinases assayed (data not shown). Interestingly, among these, **6d** particularly decreased (70%) the activity of TAK1, the TGF- β -activated kinase which is involved in the classical NF- κB pathway (see Fig. 1).

3.4.4. TAK1 inhibition

Following this result, the TAK1 dose-inhibitory potency of compounds **6a–d** were evaluated using an Invitrogen Lanthascreen® Eu Kinase Binding Assay [32]. Briefly, this assay is based on the detection of the binding of a “tracer” to a kinase by addition of a Eu-labeled anti-tag antibody. Binding of the tracer and antibody to a kinase results in a high degree of FRET, whereas displacement of the tracer with a kinase inhibitor results in a loss of FRET. The results are reported in Table 3.

As expected, staurosporine, the reference inhibitor in this assay, strongly inhibits TAK1 with an IC_{50} of 0.021 μM . From the four compounds analysed, only two, **6c** and **6d**, effectively inhibit TAK1 with an IC_{50} value of 0.58 and 2.1 μM , respectively, whereas no inhibition was observed at maximum solubility for **6a** and **6b**.

As the 3D-coordinates of TAK1 were recently available (PDB code 2EVA), [19] the molecular interactions stabilizing **6c** and **6d** inside the TAK1 cavity were analysed with a view to identify the structural elements required for their inhibitory potency.



Scheme 1. Synthesis of pyrazolo[4,3-c]isoquinolines.

Table 2

Inhibition of NIK in presence of pyrazolo[4,3-c]isoquinolines **6a–d** at 10 μM . Results are mean of 3 experiments.

Cmpd	NIK inhibition
Staurosporine	72%
6a	6%
6b	0%
6c	18%
6d	2%

Table 3

IC_{50} of pyrazolo[4,3-c]isoquinolines **6a–d** against TAK1 (N.I.=no inhibition at maximum solubility).

Cmpd	TAK1 IC_{50} (μM)
Staurosporine	0.021
6a	N.I.
6b	N.I.
6c	0.58
6d	2.1

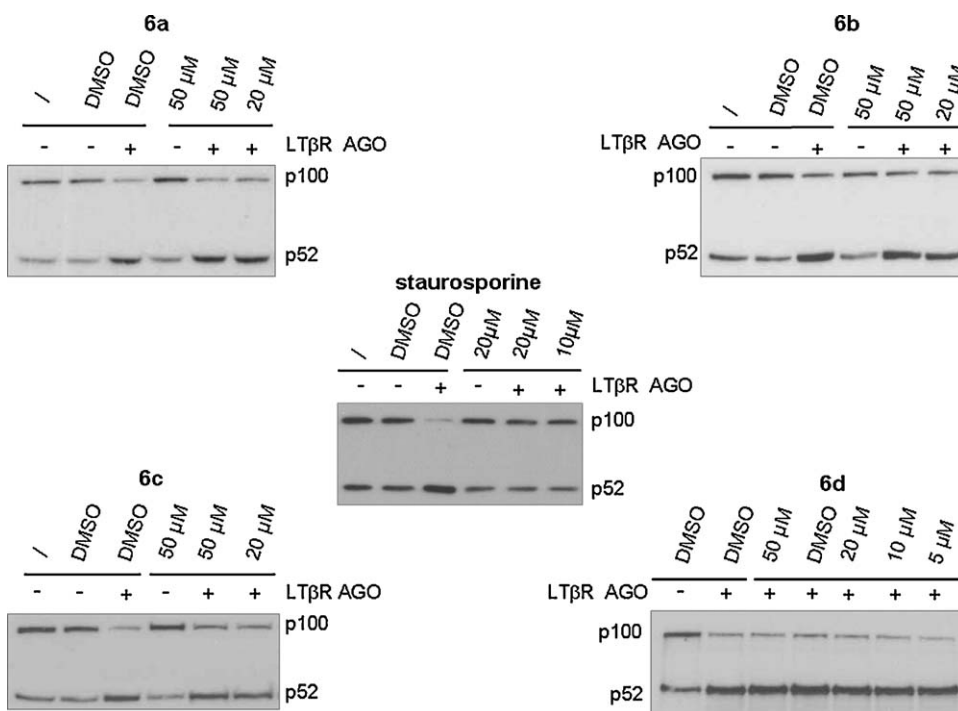


Fig. 5. Processing of p100 into p52 from HeLa cells expressing LT β R stimulated by an LT β R agonist antibody (AGO). Cells were incubated in absence or in presence of pyrazolo[4,3-c]isoquinolines **6a–d** or with staurosporine. DMSO has no effect.

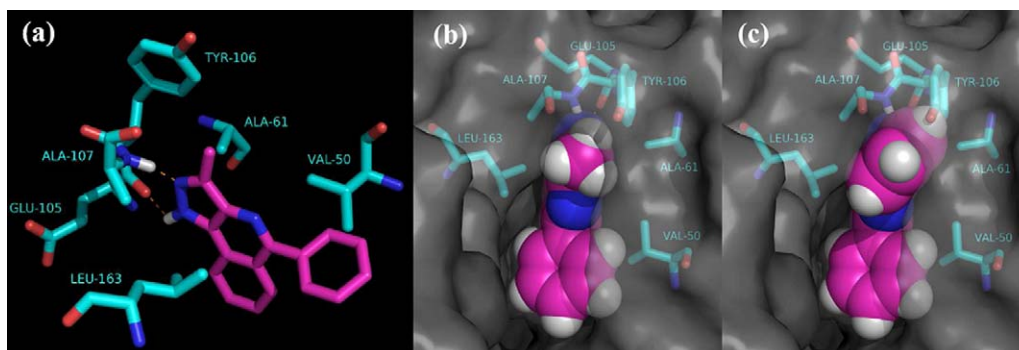


Fig. 6. Molecular interactions between (a) **6d** with stick representation, (b) **6d** and (c) **6a** with sphere representation in the hinge region of TAK1. Pictures made using PYMOL [23].

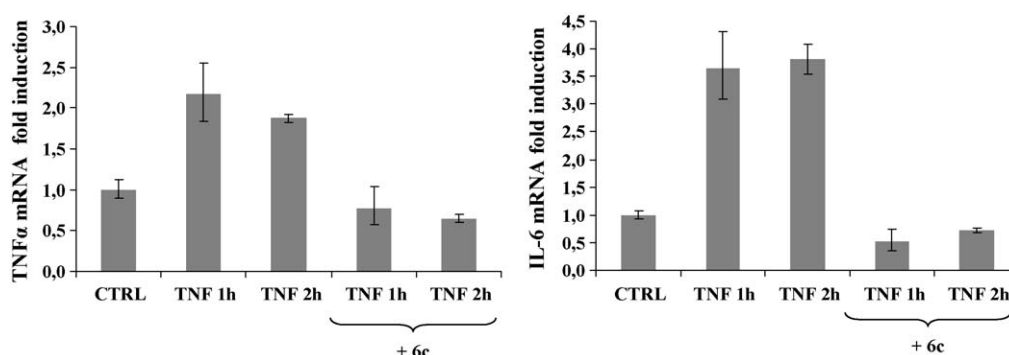


Fig. 7. Normalized TNF α and IL-6 mRNA-levels induced by TNF α (100 U/mL) in absence or in presence of TAK1 inhibitor **6c** (50 μ M). Measurements were conducted 1 h and 2 h following TNF α addition. TNF α and IL-6 mRNA-levels prior to TNF α addition (CTRL) are considered as 1. Mean \pm s.d.

When **6c** or **6d** are docked inside the TAK1 binding cleft, all of the 20 conformations adopt the same orientation with the pyrazolo[4,3-*c*]isoquinoline deeply inserted in the cavity and the R₁-methyl (see Fig. 1) pointing towards the entrance of the active site (Fig. 6a). Both compounds are stabilized by (i) two H-bonds with residues E105 and A107 in the hinge region and (ii) hydrophobic interactions with residues V50, A61 and L163 (Fig. 6a and b). Indeed, **6c** and **6d** fits perfectly the TAK1 ATP-binding site.

Interestingly, the inactivity of compounds **6a** and **6b** might be explained by a steric clash between the phenyl group in position R₁ of the pyrazolo[4,3-*c*]isoquinoline ring and the residue Y106 of TAK1 (Fig. 6c).

This study thus suggest that pyrazolo[4,3-*c*]isoquinoline are TAK1 inhibitors, at least when they are substituted in position R₁ by a methyl group (**6c–s**). When this methyl is replaced by bulkier group such as a phenyl (**6a–b**), the steric hindrance certainly prevents the compounds to bind TAK1.

3.4.5. NF- κ B classical pathway inhibition

Briefly, **6c** (50 μ M), the best TAK1 inhibitor (IC₅₀ = 0.58 μ M), was assayed using carcinoma HeLa cells stimulated by TNF α . The NF- κ B classical pathway was induced by TNF α (100 U/mL), then the levels of TNF α and IL-6 mRNA-levels were quantified in presence or in absence of **6c**. As expected (Fig. 7), TNF α doubles the relative TNF α mRNA-level 1 h (2.2-fold) and 2 h (1.9-fold) following induction, whereas the induction in presence of **6c** is only 0.77-fold and 0.65-fold respectively. TNF α strongly increases the relative IL-6 mRNA-level 1 h (3.7-fold) and 2 h (3.8-fold) after TNF α -induction. On the contrary, the addition of **6c** prevents an increase of the normalized IL-6 mRNA-levels which are 0.5-fold and 0.7-fold when measured 1 h and 2 h after induction respectively.

4. Discussion and conclusions

The initial goal of this work was to build a 3D-model of NIK to study a series of known pyrazolo[4,3-*c*]isoquinolines, claimed as NIK inhibitors, [13] with a view to elucidate the required structural elements for NIK inhibition. In the absence of any experimental structural data on this enzyme, we built a 3D-model of NIK by using comparative modeling techniques. The binding of known pyrazolo[4,3-*c*]isoquinolines was directly analysed in the putative active site. Surprisingly, this study revealed a poor binding orientation of the template inside the ATP-binding pocket of NIK. This suggested either a poor inhibitory potency or an alternative mechanism of inhibition. Based on the modeling results, we synthesized some pyrazolo[4,3-*c*]isoquinolines and characterized their inhibitory activity in two tests involving NIK: (i) an isolated enzyme assay using human recombinant NIK and (ii) a cellular assay where the alternative NF- κ B pathway only was involved. As a result, all synthesized molecules were completely deprived of any significant inhibition on both systems. On the contrary to the original patent, this confirmed these compounds were neither inhibitor of NIK nor even of the alternative NF- κ B activation pathway. To elucidate the potential target of these pyrazolo[4,3-*c*]isoquinolines, in modulating the NF- κ B pathway, a multikinase screen was performed using **6d** as example. This screening revealed interesting inhibition properties of **6d** for TAK1, a kinase which is involved in the classical NF- κ B activation pathway. This was further confirmed by determination of the inhibition (IC₅₀) of **6a–d** vs. TAK1. By preventing the increase of the TNF α and IL-6 mRNA-levels induced by TNF α , the best TAK1 inhibitor **6c** (IC₅₀ = 0.58 μ M) confirmed its ability to block the classical NF- κ B pathway.

Indeed, in the original patent, [13] the NIK inhibitory potency claimed by Flohr was based on the ability of

pyrazolo[4,3-c]isoquinolines to prevent TNF α and IL-6 release from human peripheral blood lymphocytes after stimulation by LPS or IL1 β . On the contrary, the present study demonstrated that pyrazolo[4,3-c]isoquinolines are not NIK inhibitors but are likely modulators of the classical NF- κ B pathway through TAK1 inhibition. These results are of particular importance as they allow to re-assess the mechanism of inhibition in this series. Moreover it should be noted that recent results from Tang et al. showed that conditional deletion of TAK1 in knockout mice led to multiple organ defects during development and to death after 8–10 days [29,30]. This suggests that inhibition of TAK1 is certainly not advantageous.

Finally, this study led to a reliable 3D-model of NIK that could be used to search for novel inhibitors of this enzyme.

Acknowledgments

The authors thank C. Bertolla and J. Deglim for configuring LC Methods; A-M. Murray for performing elemental analysis; C. Swijsen for designing NF- κ B activation pathways scheme; the “Fonds de la Recherche Scientifique – FNRS” for funding the Biotage SP1 Purification System; the Walloon Region for financially supporting this work (PRALTER no. 0516272). R.F. is greatly indebted to the Belgian “Fonds de la Recherche Scientifique – FNRS” for the award of a postdoctoral research grant.

Appendix A. Supplementary data

Supplementary data associated with this article can be found, in the online version, at doi:10.1016/j.bcp.2010.01.007.

References

- [1] McInnes IB, Schett G. Cytokines in the pathogenesis of rheumatoid arthritis. *Nat Rev Immunol* 2007;7(6):429–42.
- [2] Martinon F, Tschopp J. NLRs join TLRs as innate sensors of pathogens. *Trends Immunol* 2005;26(8):447–54.
- [3] Yamaguchi K, Shirakabe T, Shibuya H, Irie K, Oishi I, Ueno N, et al. Identification of a member of the Mapk family as a potential mediator of Tgf-Beta signal-transduction. *Science* 1995;270(5244):2008–11.
- [4] Sato S, Sanjo H, Takeda K, Ninomiya-Tsuji J, Yamamoto M, Kawai T, et al. Essential function for the kinase TAK1 in innate and adaptive immune responses. *Nat Immunol* 2005;6(11):1087–95.
- [5] Shim JH, Xiao C, Paschal AE, Bailey ST, Rao P, Hayden MS, et al. TAK1, but not TAB1 or TAB2, plays an essential role in multiple signaling pathways in vivo. *Genes Dev* 2005;19(22):2668–81.
- [6] Vallabhapurapu S, Karin M. Regulation and function of NF-kappaB transcription factors in the immune system. *Annu Rev Immunol* 2009;27:693–733.
- [7] Dejardin E. The alternative NF-kappaB pathway from biochemistry to biology: pitfalls and promises for future drug development. *Biochem Pharmacol* 2006;72(9):1161–79.
- [8] Vallabhapurapu S, Matsuzawa A, Zhang W, Tseng PH, Keats JJ, Wang H, et al. Non-redundant and complementary functions of TRAF2 and TRAF3 in a ubiquitination cascade that activates NIK-dependent alternative NF-kappaB signaling. *Nat Immunol* 2008;9(12):1364–70.
- [9] Liao GX, Zhang MY, Harhaj EW, Sun SC. Regulation of the NF-kappa B-inducing kinase by tumor necrosis factor receptor-associated factor 3-induced degradation. *J Biol Chem* 2004;279(25):26243–50.
- [10] Claudio E, Brown K, Park S, Wang H, Siebenlist U. BAFF-induced NEMO-independent processing of NF-kappa B2 in maturing B cells. *Nat Immunol* 2002;3(10):958–65.
- [11] Coope HJ, Atkinson PG, Huhse B, Belich M, Janzen J, Holman MJ, et al. CD40 regulates the processing of NF-kappaB2 p100 to p52. *EMBO J* 2002;21(20):5375–85.
- [12] Dejardin E, Droin NM, Delhase M, Haas E, Cao Y, Makris C, et al. The lymphotoxin-beta receptor induces different patterns of gene expression via two NF-kappaB pathways. *Immunity* 2002;17(4):525–35.
- [13] Flohr S. Pyrazoloisoquinoline derivatives as kinase inhibitors. In: *PCT Int. Appl.* US 6,841,556, 2005.
- [14] Altschul SF, Madden TL, Schaffer AA, Zhang JH, Zhang Z, Miller W, et al. Gapped BLAST and PSI-BLAST: a new generation of protein database search programs. *Nucleic Acids Res* 1997;25(17):3389–402.
- [15] Berman HM, Westbrook J, Feng Z, Gilliland G, Bhat TN, Weissig H, et al. The protein data bank. *Nucleic Acids Res* 2000;28(1):235–42.
- [16] Lambert C, Leonard N, De Bolle X, Depiereux E. ESYPred3D: prediction of proteins 3D-structures. *Bioinformatics* 2002;18(9):1250–6.
- [17] Laskowski RA. PDBsum: summaries and analyses of PDB structures. *Nucleic Acids Res* 2001;29(1):221–2.
- [18] Tripos I, SYBYL. 1699 South Hanley Rd., St. Louis, Missouri, 63144, USA.
- [19] Brown K, Vial SC, Dedi N, Long JM, Dunster NJ, Cheetham GM. Structural basis for the interaction of TAK1 kinase with its activating protein TAB1. *J Mol Biol* 2005;354(5):1013–20.
- [20] Lei M, Robinson MA, Harrison SC. The active conformation of the PAK1 kinase domain. *Structure* 2005;13(5):769–78.
- [21] Sali A, Blundell TL. Comparative protein modelling by satisfaction of spatial restraints. *J Mol Biol* 1993;234(3):779–815.
- [22] Ghose AK, Herbertz T, Pippin DA, Salvino JM, Mallamo JP. Knowledge based prediction of ligand binding modes and rational inhibitor design for kinase drug discovery. *J Med Chem* 2008;51(17):5149–71.
- [23] LCC DS, Pymol. 2008.
- [24] Ruegg UT, Burgess GM. Staurosporine, K-252 and UCN-01: potent but non-specific inhibitors of protein kinases. *Trends Pharmacol Sci* 1989;10(6):218–20.
- [25] Jones G, Willett P, Glen RC, Leach AR, Taylor R. Development and validation of a genetic algorithm for flexible docking. *J Mol Biol* 1997;267(3):727–48.
- [26] Saloutin VIYVB, Skryabina ZE, Kuzueva OG. Synthesis of fluoroalkyl-containing 2-oxyimino-1,3-dicarbonyl compounds and their reaction with hydrazine hydrate. *J Fluorine Chem* 1997;84:107.
- [27] Majid T, Hopkins CR, Pedgrift B, Collar N. Convenient synthesis of 4-amino-3,5-disubstituted pyrazoles in one-step from the corresponding diketo oximes. *Tetrahedron Lett* 2004;45(10):2137–9.
- [28] Pictet AG. Alfons, new method for the synthetic preparation of isoquinoline bases. *Berichte der Dtsch Chemischen Gesellschaft* 1910;43:2384–91.
- [29] Gaestel M, Kotlyarov A, Kracht M. Targeting innate immunity protein kinase signalling in inflammation. *Nat Rev Drug Discov* 2009;8(6):480–99.
- [30] Tang M, Wei X, Guo Y, Breslin P, Zhang S, Wei W, et al. TAK1 is required for the survival of hematopoietic cells and hepatocytes in mice. *J Exp Med* 2008;205(7):1611–9.
- [31] ³³PanQinase[®] Activity Assay performed by ProQinase, Freiburg, Germany.
- [32] Lanthascreen[®] Eu Kinase Binding Assay performed by Invitrogen Limited, Paisley, Scotland, United Kingdom.